Seismic retrofit schemes for staggered truss structures

Jinkoo Kim [a,*], Joonho Lee [a], Beomchae Kim [b]

[a] Dept. of Civil and Architectural Engineering, Sungkyunkwan University, Suwon, Republic of Korea
[b] Samsung Engineering & Construction Co., Seoul, Republic of Korea

ARTICLE INFO

ABSTRACT

In this study the seismic performances of staggered truss system (STS) structures with and without vierendeel panels were evaluated. The force–displacement relationship and seismic fragility of basic type STS were compared with those of the structures retrofitted with additional members such as interior columns, vertical cables, end braces, and buckling-restrained braces (BRB). The analysis results showed that the seismic performance of the STS with vierendeel panels could be greatly enhanced by installing interior columns. The use of end bracing and vertical cable also turned out to be somewhat effective in enhancing strength and ductility and decreasing inter-story drifts and residual displacements. Similar results were obtained in the STS structure without vierendeel panels retrofitted with end bracing or designed with some of the diagonal members replaced with BRB.

© 2015 Elsevier Ltd. All rights reserved.

1. Introduction

The staggered-truss systems (STS) consists of a series of story-high trusses spanning the total width between two rows of exterior columns and arranged in a staggered pattern on adjacent column lines. The system is known to be appropriate for use in residential buildings such as apartments, condominiums, dormitories, and hotels [1]. As columns are located only on the exterior faces of the building, large clear span and open areas can be created. Compared with conventional reinforced concrete residential buildings' plan layouts which are divided into many small spaces by vertical shear walls, the residential buildings with staggered trusses placed at alternate levels have enhanced spatial flexibility with the economy and constructability. As story-high staggered trusses function as floor beams as well as partition walls, story height can be minimized and significant advantage in economy can be achieved. Other benefits include minimum deflection and greater stiffness in the structure [2]. The reduced weight of the superstructure results in reduced seismic loads and substantial cost savings in foundation work. It was reported that the structural costs per unit building area turned out to be relatively low in STS [3]. Kim et al. [4] conducted nonlinear static analyses of staggered truss system buildings to identify failure modes under seismic loads. Zhou et al. [5] conducted a series of experimental and numerical analysis on the seismic behavior of staggered truss systems, and investigated the influence of the typical design

parameters. Chen and Zhang [6] carried out experimental research to study the failure mode and joint capacity of a steel staggered truss system model exposed to pool fire. Staggered truss systems have been successfully applied to many large-scale building projects and their efficiency and economy were reported [7–9].

To facilitate the application of the STS, AISC (American Institute of Steel Construction) published the Design Guide 14: Staggered Truss System Framing Systems [10], in which recommendations and examples for structural design are provided. The STS, however, has not been considered as one of the basic seismic-force-resisting systems in most of design codes, which implies that further research is still necessary for the system to be accepted as a standard structure system for seismic load. FEMA-450 [11] requires that seismic-force-resisting systems that are not listed as the basic seismic-force-resisting systems shall be permitted if analytical and test data are submitted to demonstrate the lateral force resistance and energy dissipation capacity. In this sense it is worthwhile to note that the special truss moment frames, which have similarity with STS in structural configuration and failure mechanism, is included in ASCE 7-13 with high response modification factor based on the extensive research on the seismic performance of the system [12–14].

In this study 6-, 12-, and 18-story staggered truss structures with vierendeel panels (Type A structures) and a 12-story structure without vierendeel panels (Type B structure) were designed, and their seismic behaviors were compared through nonlinear analysis. Fragility analyses were carried out using 44 earthquake ground records to estimate the probability of reaching specified limit states for a given earthquake intensity. Based on the analysis

* Corresponding author. Tel.: +82 31 290 7563; fax: +82 31 290 7570.
  E-mail address: jkim12@skku.edu (J. Kim).

results, seismic reinforcing schemes were derived and their effects on enhancing lateral load-resisting capacity were evaluated.

2. Design and analysis modeling of example structures

In this study total of ten STS analysis model structures were designed per current design code: 6-, 12-, and 18-story STS structures with 2 m, 2.5 m, and 3 m long vierendeel panels in the middle of the staggered trusses (Type A) and, for comparison, a 12-story STS structure without vierendeel panels (Type B). In the Type B structure it was assumed that the corridor was located outside of the structure along the longitudinal direction, which was pin-connected to the main structure and was neglected in the analysis modeling. Fig. 1 depicts the structural plan of the Type A model structures with vierendeel panel and the side view of the 6-story analysis model structure. Fig. 2 shows the elevation of the 12-story Type B model structure without vierendeel panel. The staggered trusses were located along the transverse direction, and the moment-resisting frames were placed along the longitudinal direction. No truss was placed in the first story to accommodate large open space; instead diagonal members were installed at both ends of the span along the transverse direction as was done in the example structure of the AISC Steel Design Guide [10]. Exterior columns were located in such a way that their strong axes were in parallel with longitudinal direction of the structures as recommended in the Design Guide [10]. The height of the typical stories is 3.75 m and the height of the first-story is 4.0 m.

The design loads for the model structures were determined based on the ASCE 7-10 [15] and structural member design was carried out based on the Load and the Resistance Factor Design (LRFD) of AISC 360-10 [16]. The dead load of 5.0 kN/m² and live load of 2.0 kN/m² were used as gravity loads. Along the transverse

(a) Structural plan

(b) Elevation (Line A)   (c) Elevation (Line B)

Fig. 1. Six-story staggered truss model structure with a central corridor (Type A) (mm).
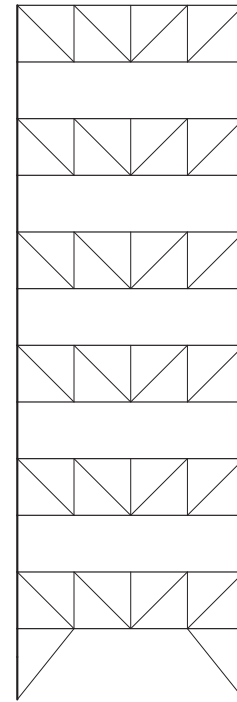

Fig. 2. 12-story staggered truss model structure without a central corridor (Type B).

direction, where staggered trusses are located, the response modification factor of 3.0 was applied in the computation of the design base shear, which is generally applied in structures not defined as one of the seismic load-resisting systems; along the longitudinal direction, where the seismic load-resisting system is the ordinary moment-resisting frames, the response modification factor of 3.5 was used. The design spectral acceleration parameters for short period (S_{DS}) and at 1.0 s (S_{D1}) are 0.5 and 0.2, respectively, and the short- and the long-period site coefficients F_a and F_v are 1.36 and 2.28, respectively. The design spectral acceleration parameters correspond to the seismic design category C_{max} and D_{min} in the ASCE 7-10 [15]. The site class was assumed to be D.

In all model structures, columns and upper and lower chords of the staggered truss were designed with A572 steel (F_y = 345 MPa, F_u = 450 MPa) and the other members were made of A500 steel (F_y = 250 MPa, F_u = 400 MPa). The columns were designed in such a way that the strength ratio P/P_{CL} is about 0.5 as was done in the design of the example structures in the AISC Steel Design Guide 14 [10], and those of the members of the staggered trusses were maintained around 0.8–0.9. The floor slabs were assumed to be rigid diaphragm in the structural analysis. Table 1 shows the fundamental natural periods of the model structures, where it can be observed that the natural period increases as the length of the vierendeel panel increases, and that the natural period of the 12-story STS without vierendeel panels is significantly smaller than that of the 12-story structure with vierendeel panels. The Type A structure is similar to the coupled shear walls connected by beams. In this case the overall stiffness depends mainly on
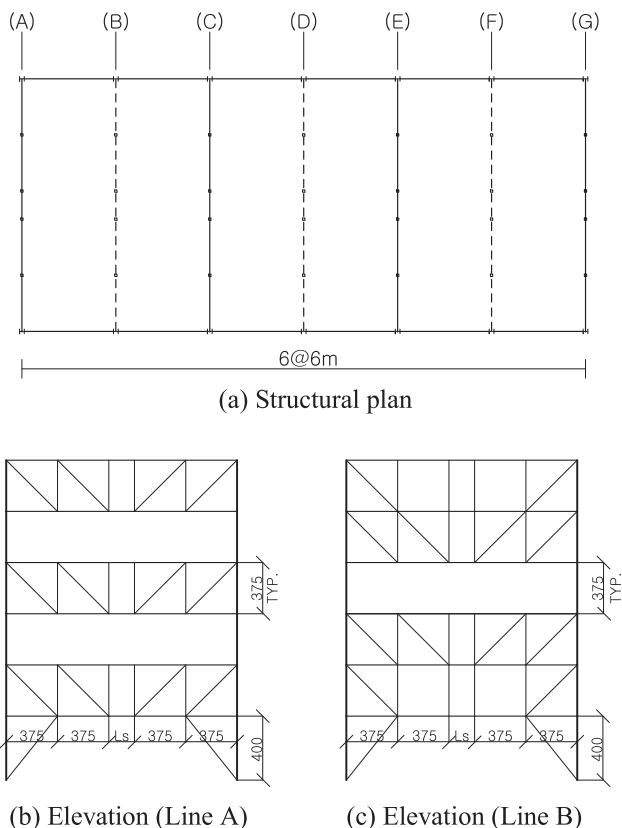
Table 1
Fundamental natural periods of the model structures.

		2 m	2.5 m	3 m
Type A	6F	1.07	1.27	1.49
	12F	1.85	2.10	2.40
	18F	2.49	2.77	3.08
Type B	12F	0.90		

the flexibility of the connecting beams. Therefore as the length of the connecting beams increases, i.e. the length of the vierendeel panel increases, the stiffness of those systems decreases and the natural period increases. The Type B structure is equivalent of the STS with zero length vierendeel panel, which results in larger stiffness and smaller natural period than the structure with finite length of vierendeel panel. The difference between the two systems can also be observed in the vibration modes of the structures depicted in Fig. 3, where the mode shape of the structure with vierendeel panels resembles that of a typical moment resisting frame due mainly to the flexibility of the vierendeel panels, whereas that of the structure without vierendeel panels is close to the mode shape of a braced frame.

3. Nonlinear analysis results

In this section nonlinear static pushover analyses were carried out to evaluate the overstrength and ductility of the model structures. Also investigated were the plastic hinge formation patterns of the model structures. The nonlinear force–displacement relationships and limit states for structural elements were defined based on the ASCE/SEI 41-06 [17]. The behaviors of structural members were defined as elastic perfectly plastic model with the expected yield stress of 1.1 times the nominal yield stress. Nonlinear static and dynamic analyses were carried out using the program code Perform-3D [18]. Fig. 4(a) and (b) show the backbone curves of selected beam and brace, respectively, with indication of the limit states such as IO (Intermediate Occupancy), LS (Life Safety), and CP (Collapse Prevention); Fig. 4(c) shows the hysteresis loop for bending behavior of beams and columns; and Fig. 4 (d) depicts the hysteresis loop for braces which has the components of (1) yield in tension, (2) buckling in compression, and (3) reloading in tension. Pushover analysis was carried out by gradually increasing the lateral load proportional to the fundamental mode shape of the structure. The following combination of gravity load was imposed on the structure during the analysis:

$$1.05 \times (\text{Dead Load}) + 0.25 \times (\text{Live Load}) \tag{1}$$

Figs. 5 and 6 show the nonlinear force–displacement relationships (pushover curves) of the model structures with and without vierendeel panels, respectively, and the various response factors obtained from the pushover curves such as yield and maximum displacements, ductility and overstrength factors are presented in Table 2. The design base shears of the model structures are also indicated on the pushover curves. The maximum displacement, δ_u, was determined as the top-story displacement when the strength drops to 80% of the maximum value ($0.8V_{max}$) as defined

in the FEMA P695 [19]. The yield displacement, δ_y, was obtained by idealizing the pushover curves as bi-linear lines as recommended in the ASCE/SEI 41 [17]. The ductility factor, μ, was obtained as the ratio of the maximum and the yield displacements, and the overstrength factor, Ω, was computed as the ratio of the maximum and the design base shears. The results show that the overstrength factor increases as the number of story increases, but that the ductility factor generally decreases as the number of story increases. As the length of the vierendeel panel increases the overstrength factor decreases but the ductility factor increases. In the 6-story structure the ductility factor increases from 2.53 to 2.78 (10% increase) as the length of vierendeel panel increases from 2 m to 3 m. The increase is 32% and 31% in the 12- and 18-story structures, respectively. This is also contributed from the increased flexibility and deformability of the longer vierendeel panels. In comparison with the 12-story structure with vierendeel panels, the 12-story structure without vierendeel panels showed higher strength and stiffness. The overstrength was computed as 7.3, which is significantly higher than those of the 12-story structures with vierendeel panels. The strength suddenly dropped at relatively small roof displacement when some diagonal members in the second and the third stories buckled under compression. However even after the first strength drop, the structure showed somewhat large residual strength and ductility. The final collapse occurred when the plastic hinge rotation of the lower story chord members exceeded the Collapse Prevention limit state.

Figs. 7 and 8 depict the plastic hinge formation of the model structures right after the strength drop. It can be observed that as the length of the vierendeel panels increases the maximum strain corresponding to each damage state also increases. In the 6- and the 12-story structure with vierendeel panels plastic hinges first formed at the chord members of the lower story vierendeel panels, and subsequently spread to adjacent beams and exterior columns. When the plastic rotation of the chord members in the vierendeel panels reached the Collapse Prevention (CP) damage state the strength dropped suddenly. In this stage plastic hinges with about 25% of CP state also formed in the nearby columns. Similar results were observed in the 18-story structure except that plastic hinges formed in the mid-height of the structure. In all model structures with middle corridor the plastic hinges formed in the vierendeel panels reached the collapse prevention limit state after the major strength drop. In the 12-story Type B structure without vierendeel panels, plastic hinges formed concentrated in the lower story truss chord members and exterior columns. Some diagonal members in the lower stories buckled which leaded to sudden drop of the overall strength of the structure.

4. Statistical seismic performance evaluation

In this section the seismic performance evaluation procedure proposed in the FEMA P695 [19] was applied to the model structures, which proposes a methodology for quantifying building system performance and response parameters for use in seismic design. Nonlinear incremental dynamic analysis results are generally used to establish the median collapse capacity and collapse margin ratio (*CMR*) for the analysis models. The ratio between the median collapse intensity, $\widehat{S_{CT}}$, and the MCE intensity, S_{MT}, is defined as the collapse margin ratio (*CMR*). The adjusted collapse margin ratio (*ACMR*) is obtained by multiplying the tabulated spectral shape factor with the collapse margin ratio that was predicted using the Far-Field record set provided by the PEER NGA Database [20]. Acceptable values of adjusted collapse margin ratio are based on total system collapse uncertainty, β_{TOT}, and established values of acceptable probabilities of collapse. They are based on the assumption that the distribution of collapse level spectral intensities is
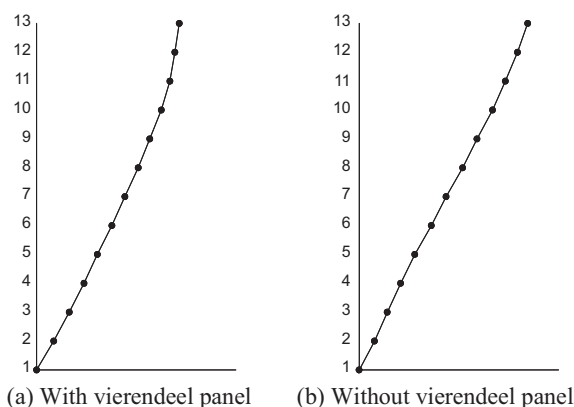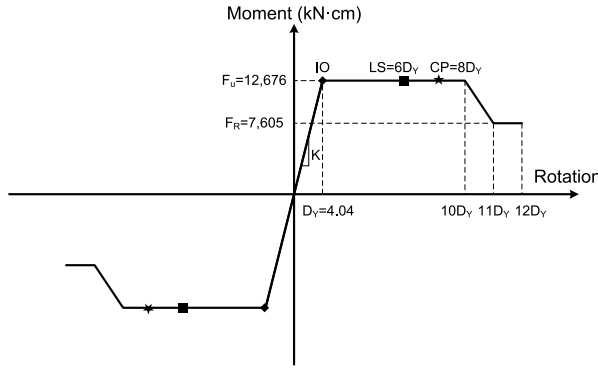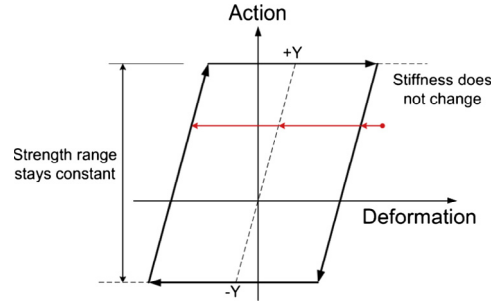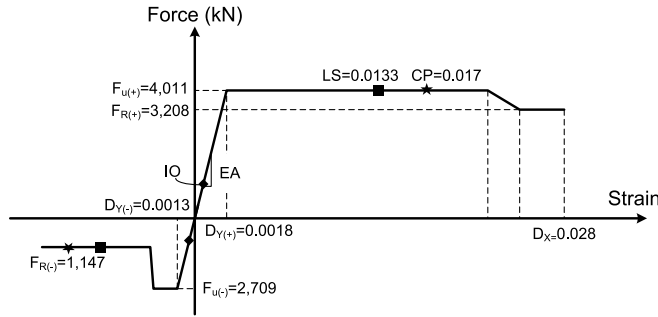

(a) With vierendeel panel (b) Without vierendeel panel

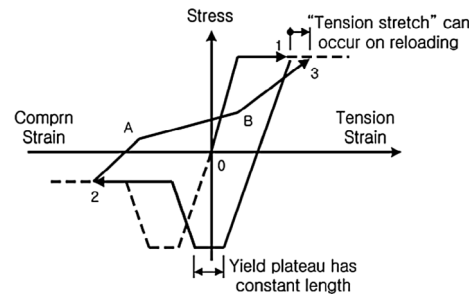**Fig. 3.** Mode shapes of 12-story STS.

(a) Beams (W8x21)

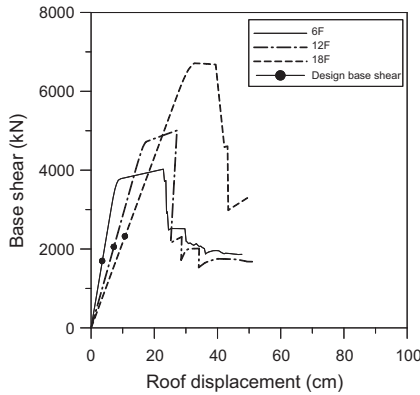(c) Hysteresis curve for bending members
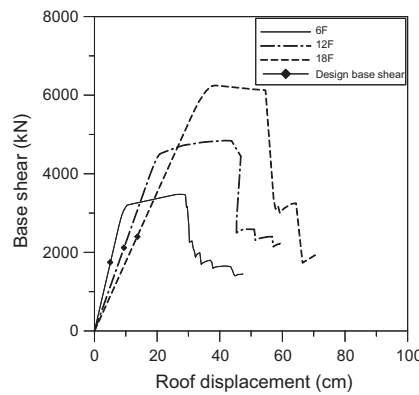
(b) Braces (HSS8x8x5/8)
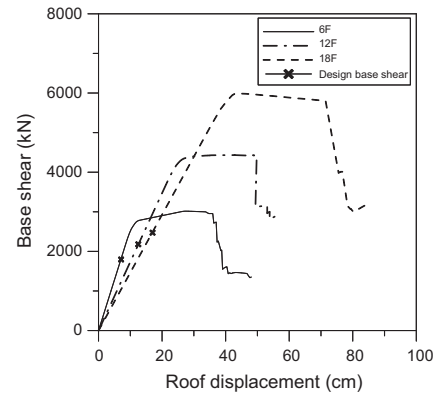
(d) Hysteresis curve for braces

Fig. 4. Nonlinear force–displacement relationship of structural members.

(a) 2m

(b) 2.5m

(c) 3m

Fig. 5. Pushover curves of Type A STS model structures having vierendeel panels with different lengths.

lognormal, with a median value, $\widehat{S_{CT}}$, and a lognormal standard deviation equal to the total system collapse uncertainty, β_{TOT}.

$$\beta_{TOT} = \sqrt{\beta_{RTR}^2 + \beta_{DR}^2 + \beta_{TD}^2 + \beta_{MDL}^2} \quad (2)$$

The total system collapse uncertainty is a function of record-to-record (RTR) uncertainty, design requirements related (DR) uncertainty, test data-related (TD) uncertainty, and modeling (MDL) uncertainty. Values of total system collapse uncertainty, β_{TOT}, and the corresponding acceptable values of adjusted collapse margin ratio, ACMR10% and ACMR20%, are provided in the FEMA P695 [19] as shown in Table 3.

The global damage states of the model structures were divided into four levels such as Slight, Moderate, Extensive, and Complete

damage as was done in the HAZUS [21]. The states of 'Slight Damage' and 'Moderate Damage' were defined as the spectral displacements corresponding to the 70% and the 100% of the yield point, respectively. The 'Extensive Damage' was defined as the quarter point from 'Moderate' to 'Complete' damage. The 'Complete Damage' was the spectral displacement at which the strength decreased to 80% of the maximum strength. Table 4 shows the maximum inter-story drift ratios of the model structures at each damage state obtained from pushover analysis.

Incremental dynamic analyses of the model structures were carried out using the twenty-two pairs of scaled records provided by the PEER NGA Database [20]. Fig. 9 shows the response spectra of the 44 earthquake records used in the incremental dynamic analyses of the 6-story model structure with 2 m vierendeel panel
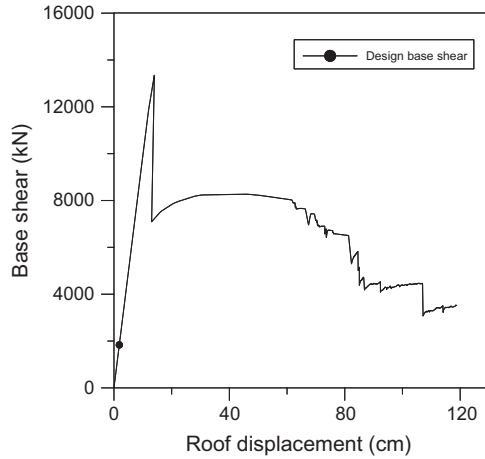
Fig. 6. Pushover curves of the 12-story Type B structure.

Table 2
Overstrength and ductility factors of the Type A model structures.

		δ_y (cm)	δ_u (cm)	μ	Ω
6F	2 m	9.42	23.80	2.53	2.37
	2.5 m	11.26	30.02	2.67	1.99
	3 m	13.40	37.24	2.78	1.65
12F	2 m	21.22	26.46	1.25	2.43
	2.5 m	25.23	44.85	1.78	2.31
	3 m	30.01	49.50	1.65	2.03
18F	2 m	34.03	41.17	1.21	2.87
	2.5 m	40.06	55.75	1.39	2.55
	3 m	46.55	74.05	1.59	2.35

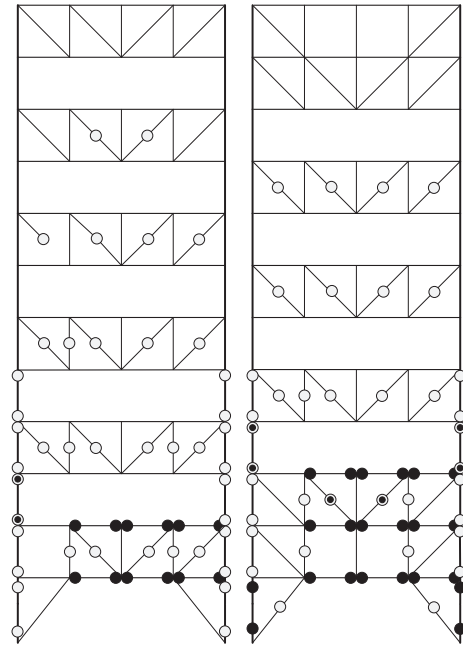**Fig. 8.** Plastic hinge formation in the 12-story Type B structure.

Table 3
Acceptable values of the adjusted collapse margin ratios (ACMR$_{10\%}$ and ACMR$_{20\%}$).

Total system collapse uncertainty	Collapse probability				
	5%	10% (ACMR$_{10\%}$)	15%	20% (ACMR$_{20\%}$)	25%
⋮	⋮	⋮	⋮	⋮	⋮
⋮	⋮	⋮	⋮	⋮	⋮
0.675	3.04	2.38	2.01	1.76	1.58
0.700	3.16	2.45	2.07	1.80	1.60
0.725	3.30	2.53	2.12	1.84	1.63
0.750	3.43	2.61	2.18	1.88	1.66
0.775	3.58	2.70	2.23	1.92	1.69
0.800	3.73	2.79	2.29	1.96	1.72
0.825	3.88	2.88	2.35	2.00	1.74
⋮	⋮	⋮	⋮	⋮	⋮
⋮	⋮	⋮	⋮	⋮	⋮

for all vibration modes, and the spectral acceleration *vs.* maximum inter-story drift ratio was plotted. Figs. 10 and 11 depict the incremental dynamic analysis results of the model structures with and without vierendeel panels, respectively. Table 5 shows the adjusted collapse margin ratios (ACMR) of the Type A models with 2 m vierendeel panel and the structure without vierendeel panel obtained from the IDA curves and the corresponding acceptable values provided in the FEMA P695 [19]. It can be noticed that the median collapse intensity, $\widehat{S_{CT}}$, generally decreases as the number of story increases. However as the MCE intensity, S_{MT}, also decreases as the number of story increases, the collapse margin ratio, which is the ratio of the two values, seems to be independent of the building height. It also can be observed that the adjusted collapse margin ratios of the model structures were larger than the acceptable values of *ACMR20%*. This implies that the parameters used in the seismic design of the model structures are valid.

The seismic fragility is described by the conditional probability that the structural capacity, *C*, fails to resist the structural demand, *D*, given the seismic intensity hazard, *SI*, and is modeled by a lognormal cumulative distribution function as follows [22]:

$$P[D \geq C] = \Phi\left(\ln\left[D/\widehat{C}\right]/\beta_C\right) \tag{3}$$

Fig. 7. Plastic hinge formation in the Type A structures.

(a) 6-story   (b) 12-story   (c) 18-story

length. They were scaled in such a way that the spectral acceleration of each record at the fundamental period of the structure, which is 1.07 s, becomes 1.0 g. Damping ratios of 5% were used

Table 4
Maximum inter-story drift ratio of model structures at each damage state.

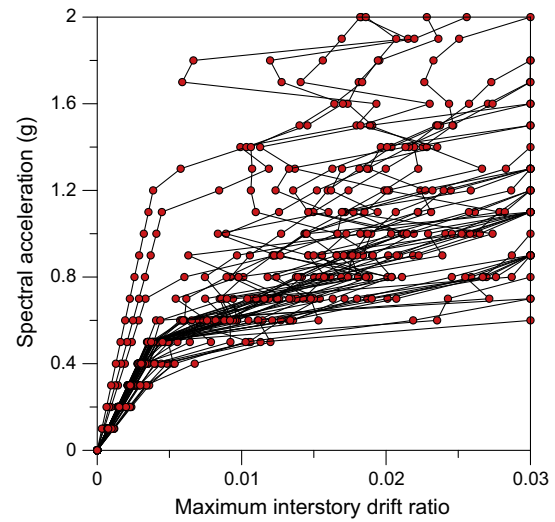|		Slight	Moderate	Extensive	Complete
Type A	6F_2m	0.0044	0.0066	0.0094	0.0179
	6F_2.5m	0.0054	0.0079	0.0113	0.0212
	6F_3m	0.0063	0.0094	0.0140	0.0283
	12F_2m	0.0051	0.0103	0.0111	0.0193
	12F_2.5m	0.0057	0.0108	0.0139	0.0217
	12F_3m	0.0061	0.0110	0.0141	0.0219
	18F_2m	0.0044	0.0085	0.0096	0.0127
	18F_2.5m	0.0050	0.0088	0.0110	0.0172
	18F_3m	0.0058	0.0109	0.0152	0.0274
Type B	12F	0.0026	0.0078	0.0146	0.0379

Fig. 11. Incremental dynamic analysis results of the 12-story Type B structure.

Fig. 9. Response spectra of the 44 scaled ground motions scaled to the fundamental period of 1.07 s.

where $\Phi[\cdot]$ = Standard normal probability integral, $\widehat{C}$ = median structural capacity, associated with the limit state, and β_C = uncertainty in C. The median structural capacity $\widehat{C}$ associated with each damage limit state was obtained from the IDA curves as the spectral acceleration at which the limit state was reached

by at least 22 earthquake records. Table 6 shows the median structural capacity $\widehat{C}$ associated with the four limit states obtained from the incremental dynamic analysis results of the 44 earthquake records. It can be seen that in all damage states the median capacity decreases as the number of story increases and the length of vierendeel panel increases. It also can be observed that the median capacity of the 12-story structure without vierendeel panels, which has significantly larger stiffness than that of the structure with vierendeel panels, is more than three times larger than those of the structures with vierendeel panels.

Figs. 12 and 13 depict the fragility curves of the analysis model structures with and without vierendeel panels, respectively, corresponding to the four damage states described above. They provide the probability of exceeding a prescribed level of damage for a wide range of ground motion intensities. For the uncertainty associated with the structural capacity, β_C, to be used in the normal probability integral function (Eq. (3)), the total system collapse uncertainty, β_{TOT}, shown in Eq. (2) was used. The total system collapse uncertainty was estimated to be 0.731 based on the FEMA P-695 using the values β_{RTR} (record-to-record uncertainty) = 0.2 (minimum value), β_{DR} (design requirements-related

(a) 6 story   (b) 12 story   (c) 18 story
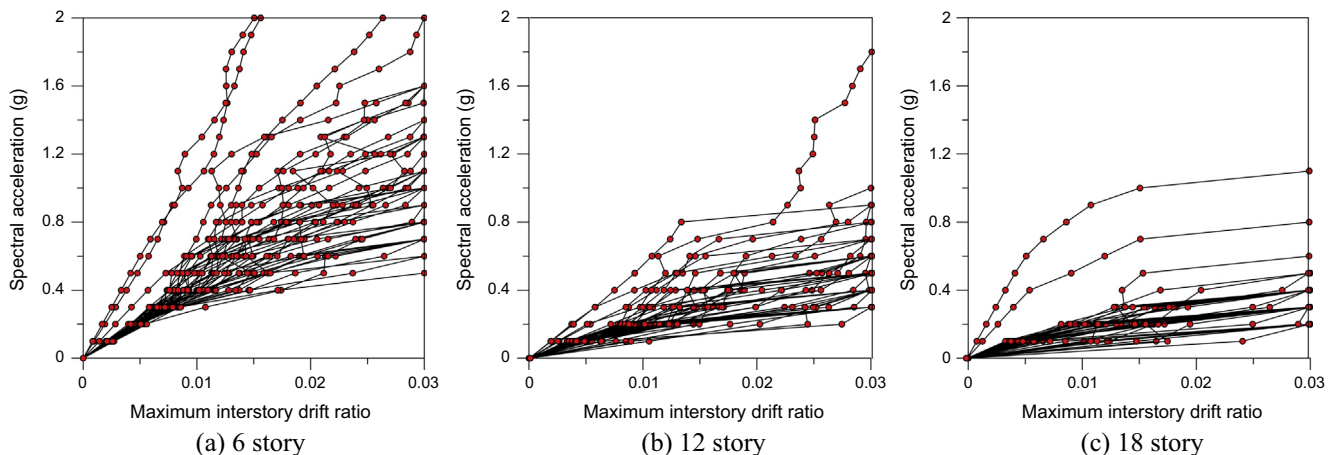
Fig. 10. Incremental dynamic analysis results of the structures with 2 m-wide middle corridor.

Table 5
Adjusted collapse margin ratios of the Type A (2 m vierendeel panels) and Type B structures.

	Story	$\hat{S}_{CT}$	S_{MT}	CMR	SSF	ACMR	$ACMR_{20\%}$	Pass/Fail
Type A	6	0.95 g	0.275 g	3.455	1.125	3.389	1.85	Pass
	12	0.68 g	0.159 g	4.277	1.068	4.567	1.85	Pass
	18	0.35 g	0.119 g	2.941	1.065	3.132	1.85	Pass
Type B	12	0.70 g	0.329 g	2.128	1.015	2.344	1.85	Pass

Table 6
Median structural capacity $\hat{C}$ associated with the limit states (g).

		Slight	Moderate	Extensive	Complete
Type A	6F_2m	0.19	0.28	0.38	0.70
	6F_2.5m	0.17	0.25	0.37	0.63
	6F_3m	0.14	0.21	0.33	0.61
	12F_2m	0.12	0.20	0.25	0.40
	12F_2.5m	0.11	0.19	0.24	0.37
	12F_3m	0.10	0.15	0.19	0.28
	18F_2m	0.09	0.15	0.16	0.19
	18F_2.5m	0.05	0.09	0.13	0.16
	18F_3m	0.05	0.09	0.11	0.15
Type B	12F	0.34	0.58	0.76	1.38

uncertainty) = 0.35 (Fair), β_{TD} (test data-related uncertainty) = 0.5 (Poor), and β_{MDL} (modeling uncertainty) = 0.35 (Fair). It can be observed that the probability of reaching each damage state increases as the number of story and the length of the vierendeel panel increase. Among the four damage states considered, the increase in the failure probability for the Collapse damage state is more predominant than the other limit states. In the 6-story structure with 2 m vierendeel length, the probabilities of reaching the Slight and the Moderate damage states exceed 0.9 when the spectral acceleration reaches 1.0 g, while the probability of reaching the Collapse state is below 0.7. At the same acceleration level, the Collapse probability increases to 0.89 and 0.98 as the number of story increases to 12 and 18, respectively. In the 12-story structures the Collapse probability increases from 0.89 to 0.96 as the length of vierendeel panel increases from 2 m to 3 m, respectively. In comparison with the structure with vierendeel panels, the structure without vierendeel panels shows much smaller probability of reaching each damage state. The decrease in the probability for reaching the Collapse state turned out to be the most significant.

5. Seismic retrofit schemes for staggered truss systems

5.1. Retrofit of the structure with vierendeel panels

It was observed in the previous section that the STS model structures have sufficient stiffness and strength but have relatively small ductility, especially in the 12- and 18-story structures, as a result of damage concentration in the lower story vierendeel panels (in Type A STS with middle corridor) or in truss diagonal members (in Type B STS without middle corridor). In this section the effects of some seismic retrofit schemes for the STS structures were investigated. Three retrofit schemes were considered in the 12-story structure with 2.5 m wide vierendeel panels.

The first scheme is to add interior columns along both sides of the middle corridor which passes through the vierendeel panels as shown in Fig. 14(a). This scheme reduces the span of the trusses to less than half of the original length and is expected to enhance the redundancy of the structure significantly. The interior columns

may be enclosed inside of the partition walls located along the middle corridor. However one of the main advantages of STS, which is to provide column free large open space in the first story, is lost. In addition additional footings are required for the internal columns and the columns may not be small enough to be hidden inside of the partition walls. The added columns are rigidly connected to the chord members of the staggered trusses in case of retrofit of existing structures. However if the interior columns are considered for new structures, they are vertically continuous and the staggered trusses are pin connected to the interior (and the exterior) columns and the vierendeel panels are rigidly connected to the interior columns. The second scheme is to add a diagonal bracing between upper and lower staggered trusses at both ends of all the stories without trusses as shown in Fig. 14(b). In the original structure the end braces are installed only in the first story. In the third scheme tension members such as cables or steel rods were added from the top story to the second story at both sides of the middle corridor, as shown in Fig. 14(c), with the intention that they might function like zipper columns in a structure with chevron braces. The cables/rods have advantage in that they are not required in the first story and, as they generally have smaller cross section than typical steel columns, they can easily be concealed inside of partition walls and may not interfere with spatial planning. The size of the cable is determined in such a way that the internal potential energy of the cable is larger than the energy stored in the truss right below the cable when the system is displaced to the limit state due to lateral load as shown in Fig. 15. It was assumed that plastic hinges were concentrated at the ends of the chord members in the vierendeel panel. In the figure the angle φ of the deformed configuration can be obtained as follows:

$$\varphi = \frac{\pi}{2} + \frac{L}{L_s}\theta \tag{4}$$

where L_s is the length of the vierendeel panel and L is the overall length of the staggered truss. The final length of the elongated cable is $l_2 + l_3$ which are obtained as follow from the deformed configuration:

$$l_2 = \frac{h}{\cos\theta}; \quad l_3 = \frac{L - L_s}{2}\tan\theta \tag{5}$$

The elongation of the cable, Δl, is obtained as the difference between the original length and the final length:

$$\Delta l = l_2 + l_3 - l_1 = \frac{(L - L_s)\sin\theta + 2h}{2\cos\theta} - h \tag{6}$$

If θ is very small (say less than 0.05) then $\sin\theta \cong \theta$ and $\cos\theta \cong 1$. Therefore Δl can be simplified as follows:

$$\Delta l = \frac{(L - L_s)}{2}\theta \tag{7}$$

The minimum required cross sectional area of the cable was obtained based on the condition that the energy stored in the cable is equal to the energy stored in the four plastic hinges in the vierendeel panel:
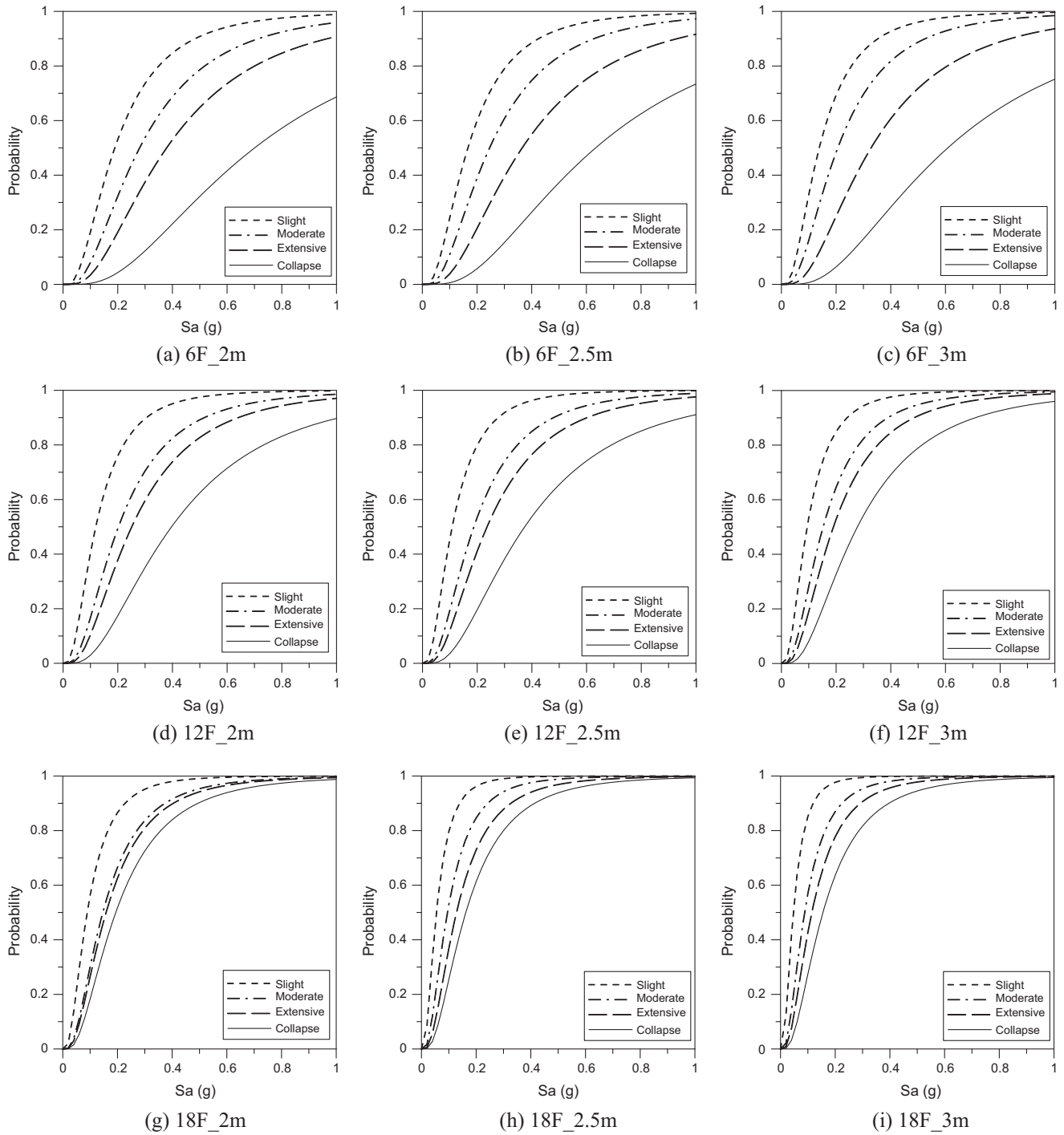
Fig. 12. Fragility curves of the Type A model structures with various length of vierendeel panel.

$$A_c F_{yc} \Delta l \geq 4 M_p \theta \qquad (8)$$

$$A_c \geq \frac{4 M_p}{F_{yc} \Delta l} \theta \qquad (9)$$

where A_c is the minimum required cross sectional area of a cable, F_{yc} is the yield strength of the cable, and M_p is the plastic moment of the vierendeel panel chord members. In this way the cables can be designed not to yield when subjected to design level seismic load.
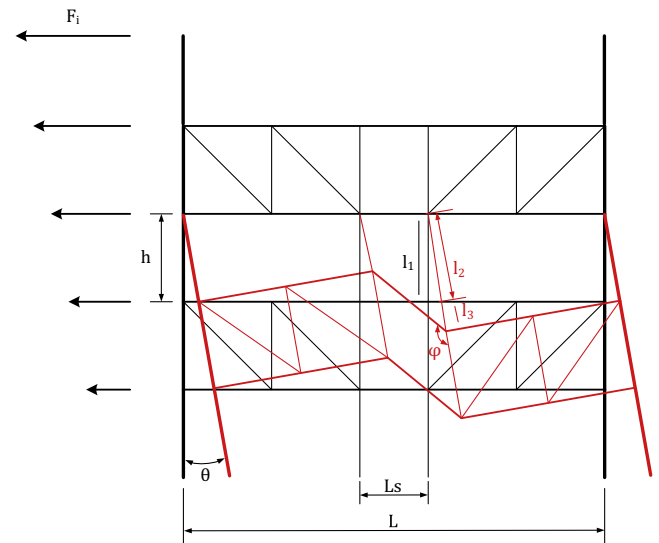
The retrofit schemes were applied to the 12-story original structure with 2.5 m long vierendeel panels and the revised structures were redesigned using the same design loads. Table 7 shows the selected member size of the original and the retrofitted structures at the selected stories. The size of the added interior columns varied from HSS10 × 10 × 1/2 (in) to HSS8 × 8 × 3/16. It was observed in the structure with added interior columns that the sizes of the truss chord members decreased slightly as a result of reduced span length, and in the structure with added end bracing the sizes of exterior columns and diagonal members directly connected to the added bracing were slightly reduced. The use of Eq. (9) resulted
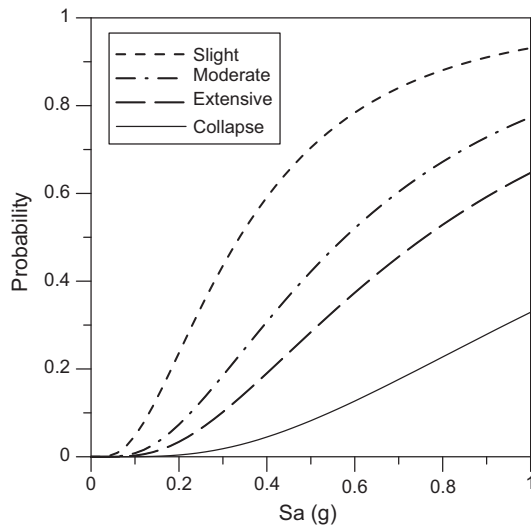
Fig. 13. Fragility curves of the 12-story Type B model structure without vierendeel panels.

Fig. 15. Deformed configuration of a Type A structure reinforced with cables.

in the required cable diameter of 4 cm to 2 cm in the model structure depending on the stories. Compared with the amount of steel in the original structure, the required steel for the first (addition of interior columns) and the second (addition of end bracing) retrofit schemes increased by 9.5% and 1.9%, respectively. The amount of the cable added to the structure is 0.7% of the total weight of the structural steel. Fig. 16 shows the pushover curves of the 12-story STS structure with and without application of the retrofit schemes, and various response factors such as displacement at yield, maximum displacement, ductility ratio, and overstrength factors are presented in Table 8. It was observed that the overstrength and ductility of the model structure retrofitted with interior columns are respectively 167.7% and 239.7% higher than those of the original structure. The structure reinforced with end bracing showed 13.6% and 42.8% higher overstrength and ductility factors,
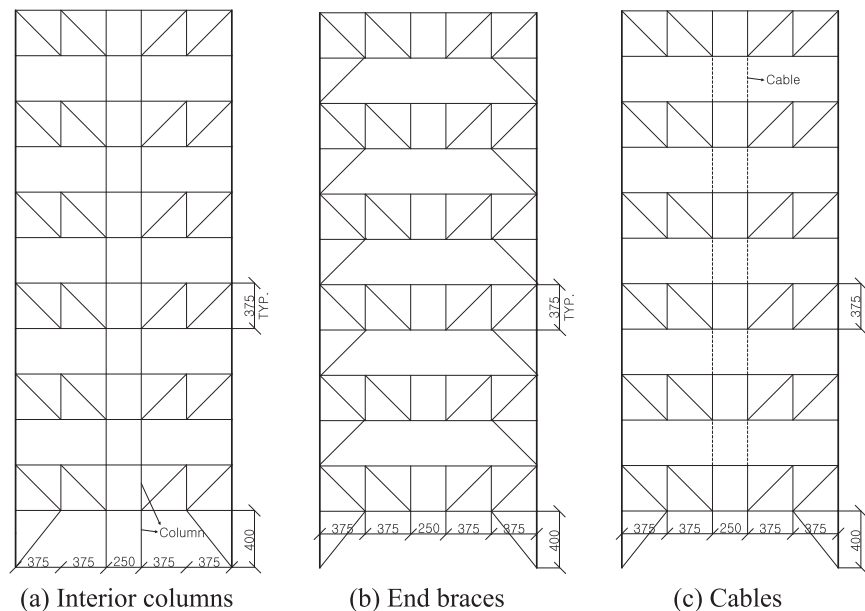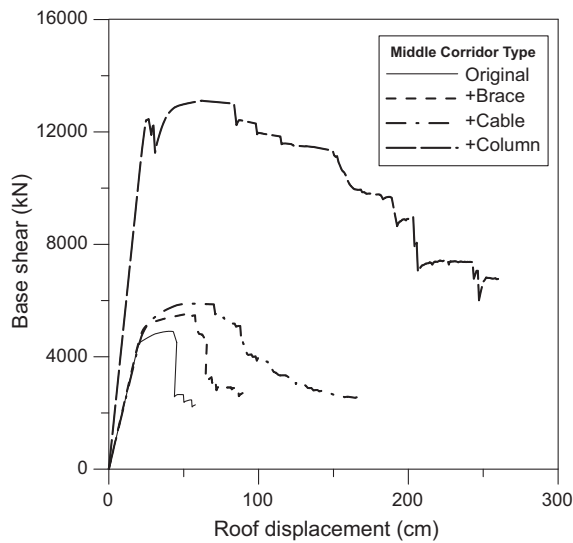
Table 7
Selected member size of the retrofitted 12-story structure with 2.5 m vierendeel panel (unit: in).

Story	Model	Column	Chord	Diagonal	Vertical
2	Original	W12 × 190	W8 × 35	HSS8 × 8 × 5/8	HSS8 × 8 × 1/2
	Column	W12 × 190	W8 × 21	HSS8 × 8 × 5/8	HSS10 × 10 × 1/2
	Brace	W12 × 190	W8 × 35	HSS8 × 8 × 1/2	HSS8 × 8 × 1/2
12	Original	W12 × 53	W8 × 21	HSS8 × 8 × 1/2	HSS8 × 8 × 1/2
	Column	W12 × 53	W8 × 21	HSS8 × 8 × 1/2	HSS8 × 8 × 1/2
	Brace	W12 × 50	W8 × 21	HSS6 × 6 × 1/2	HSS8 × 8 × 1/2

respectively. In the structure with added cables, the overstrength and ductility factors increased by 20.5% and 77.4%, respectively. Fig. 17 depicts the plastic hinge formation in each retrofitted

(a) Interior columns   (b) End braces   (c) Cables

Fig. 14. Seismic reinforcing schemes for Type A structures.

Fig. 16. Pushover curves of the 12-story Type A structure retrofitted with various methods.
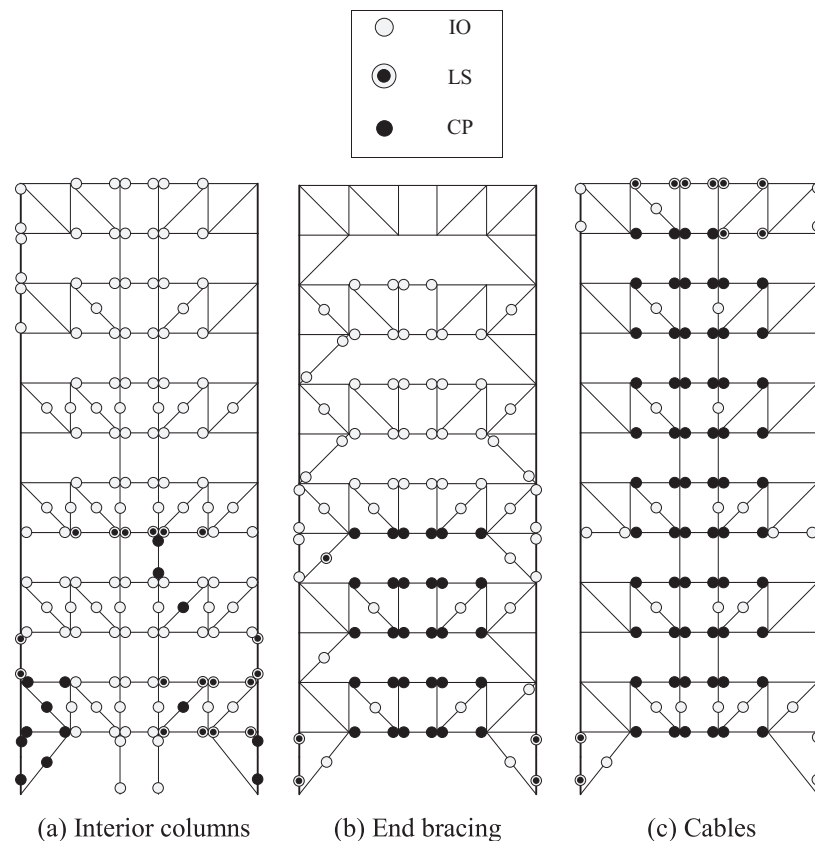
Table 8
Overstrength and ductility factors of the retrofitted Type A structures.

	δ_y (cm)	δ_u (cm)	μ	Ω
Original	25.87	44.85	1.73	2.31
Column	26.81	157.87	5.89	6.17
Brace	26.43	65.41	2.47	2.62
Cable	28.69	88.23	3.08	2.78

structure right after major strength drop. In the structure retro-fitted with interior columns plastic hinges formed concentrated in the columns, diagonal members, and chord members in the lower stories. Some plastic hinges formed in the exterior columns and diagonal members reached the collapse prevention (CP) limit state, and the plastic rotation of the plastic hinges in the vierendeel panels is less than 50% of the CP limit state. The major strength drop occurred due to the buckling of diagonal members and the plastic hinge formation in the exterior columns. In the structure with added end bracing plastic hinges formed mainly in the low to mid-story chord members. It was observed that the collapse was initiated when plastic hinges in the lower story chord members reached the CP state. In the structure retrofitted with cables plastic hinges were widely distributed throughout the building height, and the collapse started when plastic hinges formed in the lower story vierendeel panels reached the CP limit state.

Even though not shown in this paper, the addition of interior columns from the second to the top stories resulted in similar pushover curve and plastic hinge formation to those of the structure retrofitted with cables. In this case the increase in the structural steel is 10.1%, which is slightly larger than the amount of steel required for the first retrofit scheme (added columns in all stories). It was observed that when interior columns are not placed in the first story the decrease in the size of chord members in the staggered trusses is not significant.

Fig. 18 shows the mean maximum inter-story drifts and residual top story displacements of the 12-story model structures obtained from nonlinear dynamic analyses using the seven earthquake records shown in Table 9 scaled to the maximum considered earthquake spectrum of Los Angeles area ($S_g = 1.61$, $S_1 = 0.79$). It can be observed that the mean seismic responses of the original

(a) Interior columns   (b) End bracing   (c) Cables

Fig. 17. Plastic hinge formation in the 12-story Type A structure at the point of major strength drop after retrofit.

(a) Inter-story drift ratios
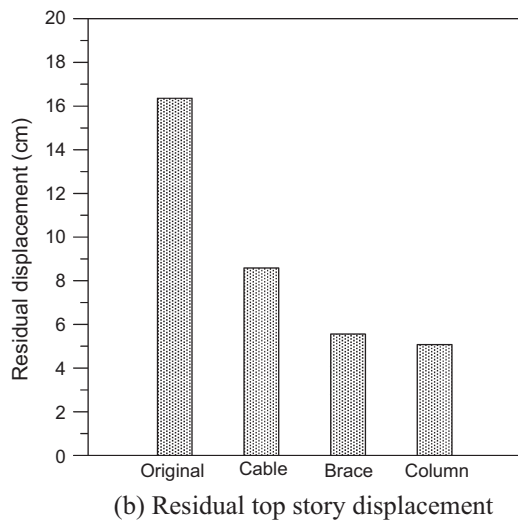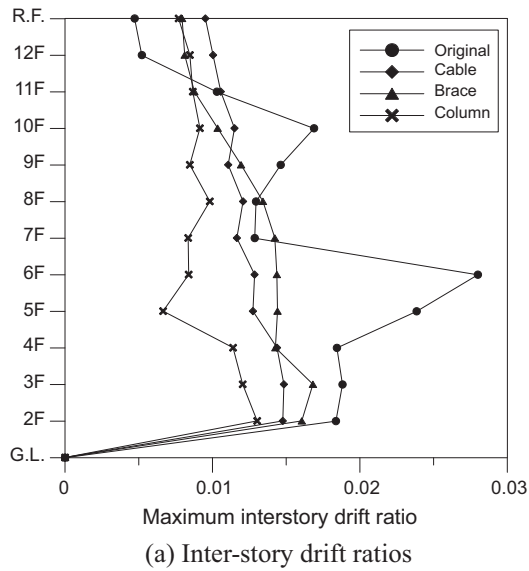

(b) Residual top story displacement

Fig. 18. Mean responses of the 12-story Type A structures subjected to strong earthquakes.

Table 9
Earthquake records used in the dynamic analysis.

Name	M	Year	PGA (g)	PGV (cm/s)
Northridge	6.7	1994	0.52	63
Imperial Valley	6.5	1979	0.38	42
Kobe, Japan	6.9	1995	0.51	37
Kocaeli, Turkey	7.5	1999	0.36	59
Manjil, Iran	7.4	1990	0.51	54
Superstition Hills	6.5	1987	0.45	36
San Fernando	6.6	1971	0.21	19

Table 10
Limit states for the maximum inter-story drift ratio of the 12-story Type A structures after retrofit at each damage state.

	Slight	Moderate	Extensive	Complete
Original	0.0057	0.0108	0.0139	0.0217
Column	0.0053	0.0069	0.0092	0.0155
Brace	0.0055	0.0094	0.0126	0.0206
Cable	0.0061	0.0090	0.0111	0.0161

Table 11
Median structural capacity $\widehat{C}$ for the Type B structures associated with the global limit states after retrofit (g).

	Slight	Moderate	Extensive	Complete
Original	0.11	0.19	0.24	0.37
Column	0.31	0.42	0.56	0.84
Brace	0.11	0.18	0.26	0.46
Cable	0.13	0.19	0.25	0.52

structure were significantly reduced in the retrofitted structures. The maximum inter-story drift of the original structure is largest due to the concentration of damage in a few stories as can be observed in Fig. 7. On the other hand, plastic hinges are more widely distributed throughout the stories in the retrofitted structures, as shown in Fig. 17, which results in smaller maximum inter-story drift even though the roof displacements are larger than that of the original structure. The reduced inter-story drifts in the retrofitted structures also contributed to the significant
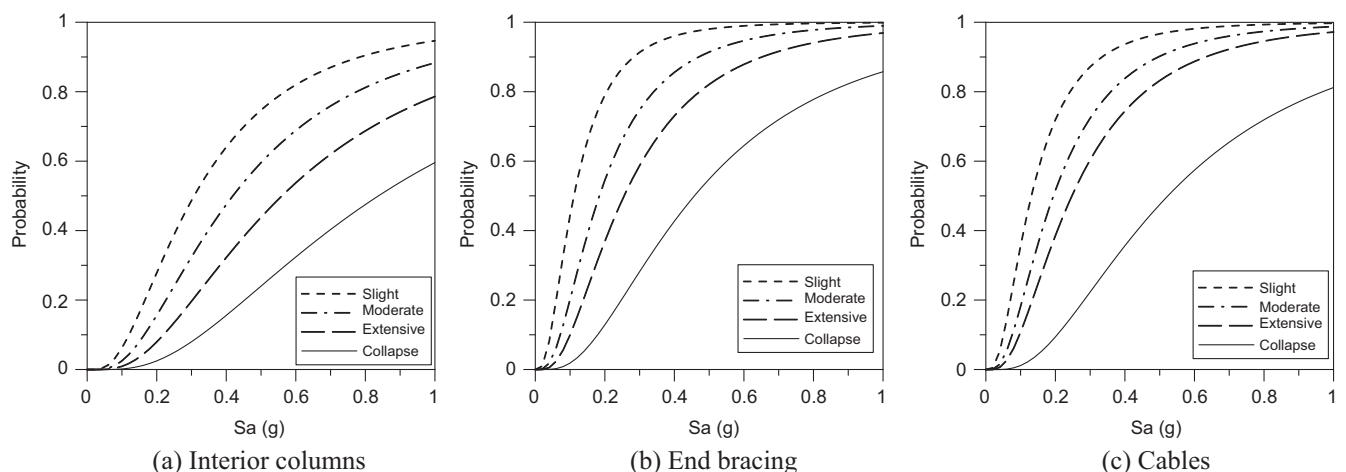

(a) Interior columns

(b) End bracing

(c) Cables

Fig. 19. Fragility curves of the 12-story Type A structures retrofitted with various methods.

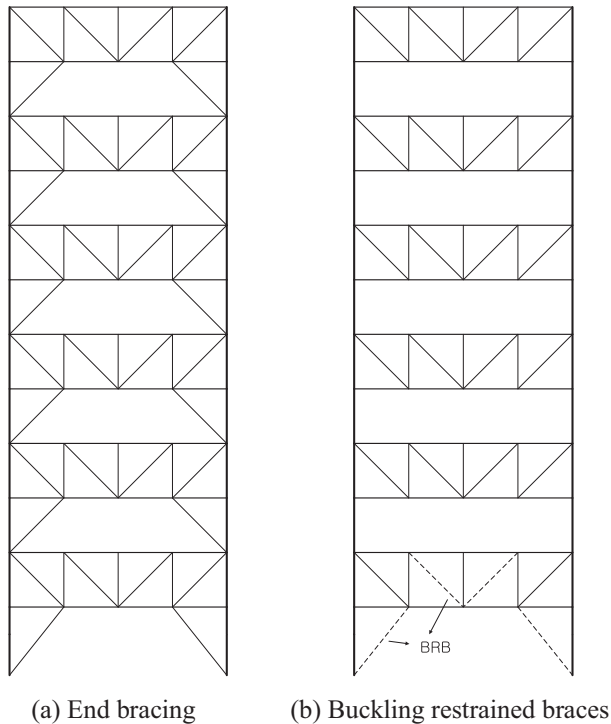(a) End bracing   (b) Buckling restrained braces

Fig. 20. Retrofit schemes for Type B structure.

reduction of residual displacement. This implies that the time and cost required for repair will be greatly reduced.

Fig. 19 depicts the fragility curves of the 12-story Type A model structures retrofitted by three different methods obtained from incremental dynamic analyses using the 44-records previously used. The limit states for inter-story drifts corresponding to the four different global damage states obtained from pushover analysis are presented in Table 10. The median structural capacities associated with each limit state, $\widehat{C}$, obtained from incremental dynamic analysis results are shown in Table 11. It can be observed that the seismic fragilities, which are the probability of reaching the given limit states, of the structure with additional end bracing for the 'Slight' and 'Moderate' damages are similar to those of the original structure, whereas the fragility for the 'Complete' damage state decreased slightly. Similar results were obtained in the structure with added cables along the corridor except that the fragility for the 'Complete' damage state further decreased. In the structure retrofitted with interior columns the probabilities of reaching all four damage states decreased significantly compared with those of the original structure, which is consistent with the significant increase in the pushover curve of the structure. Based on the fragility analysis results it can be concluded that the staggered truss structures with added end bracing or interior vertical tension members such as cables may be more effective in preventing total collapse against large earthquake than in reducing damage for moderate earthquakes.

5.2. Retrofit of the structure without vierendeel panels

It was observed in the pushover analysis results described in Fig. 6 that, even though the Type B structure without vierendeel panels had higher strength, the strength dropped suddenly at relatively small roof displacement due to the buckling of some diagonal members in the lower story trusses. It was also observed that plastic hinges were concentrated in the lower story truss chord members and exterior columns, which diminishes the effective use of structural elements when it is subjected to seismic loads. In this section two methods were applied to enhance the seismic performance of the structure. In the first method, the end braces were applied again in every story as depicted in Fig. 20(a). In the second method, based on the observation that the sudden strength drop was caused by buckling of a few truss diagonal members, some critical braces were replaced by buckling-restrained braces (BRB). The locations of the BRB are shown as dotted lines in Fig. 20(b). The configuration and the hysteresis curve of the BRB used in the analysis are depicted in Fig. 21 [23], and Fig. 22 depicts the idealized skeleton curve of the BRB used in the analysis. The tension strength adjustment factor ω and the compression strength adjustment factor β of the idealized skeleton were obtained as 1.2 from the experimental hysteresis curve, and the fracture strain was assumed to be 12 times the yield strain which is slightly smaller than the fracture point obtained from the experiment.

When the model structure was redesigned with added end braces the overall amount of steel was slightly reduced. In case BRB were applied in the selected locations and redesigned, the cross-sectional area of the BRB core elements was reduced to about 35% of that the original brace members. However the change in the total weight of structural steel is minute due to the addition of the exterior steel tubes of the BRB which only works to prevent buckling of the core members. Fig. 23 depicts the pushover curves and Table 12 shows the seismic response factors of the retrofitted Type B structures. It can be found that the overstrength and the ductility factors of the structure retrofitted with end bracing increased by 4.78% and 13.84%, respectively, compared with those of the original structure. The residual strength after the first strength drop increased by 35%. In the structure retrofitted with BRB, global yielding started at significantly lower strength, and the maximum strength of the structure decreased by 9.8% due to the reduced size of the BRB core elements compared with the size of the conventional braces. However compared with the somewhat brittle behavior of the original structure and the structure with end braces, the structure with BRB behaved in more ductile manner. The overall strength of the structure with BRB dropped after significant inelastic deformation due mainly to the large deformation capacity of the BRB. The plastic hinge formation of the retrofitted structures at the Collapse stage is shown in Fig. 24. It was observed in the structure with end braces that the strength first dropped due to buckling of the lower story diagonal members and the final collapse was initiated by the failure of the truss chord members. Compared with the plastic hinge deformation in the original structure shown in Fig. 8, the amount of plastic deformations in lower story columns and bracing of the retrofitted structures are significantly reduced and most severe damages are concentrated in the second story chord members. The number of plastic hinges in the bracing members in the upper stories also somewhat decreased. This change in plastic hinge formation pattern resulted in the significant increase in overall ductility as can be observed in Fig. 23. In the structure retrofitted with end bracing, strength suddenly dropped when some diagonal members in the lower story staggered trusses buckled; however the amount of strength drop was somewhat reduced since the damage was distributed to the added end bracing. In the model structure retrofitted with BRB, plastic hinges first formed in the BRB followed by formation of plastic hinges at the chord members and columns in the lower stories. After significant plastic deformation had occurred, the excessive plastic deformation in the first story columns leaded to collapse of the structure.
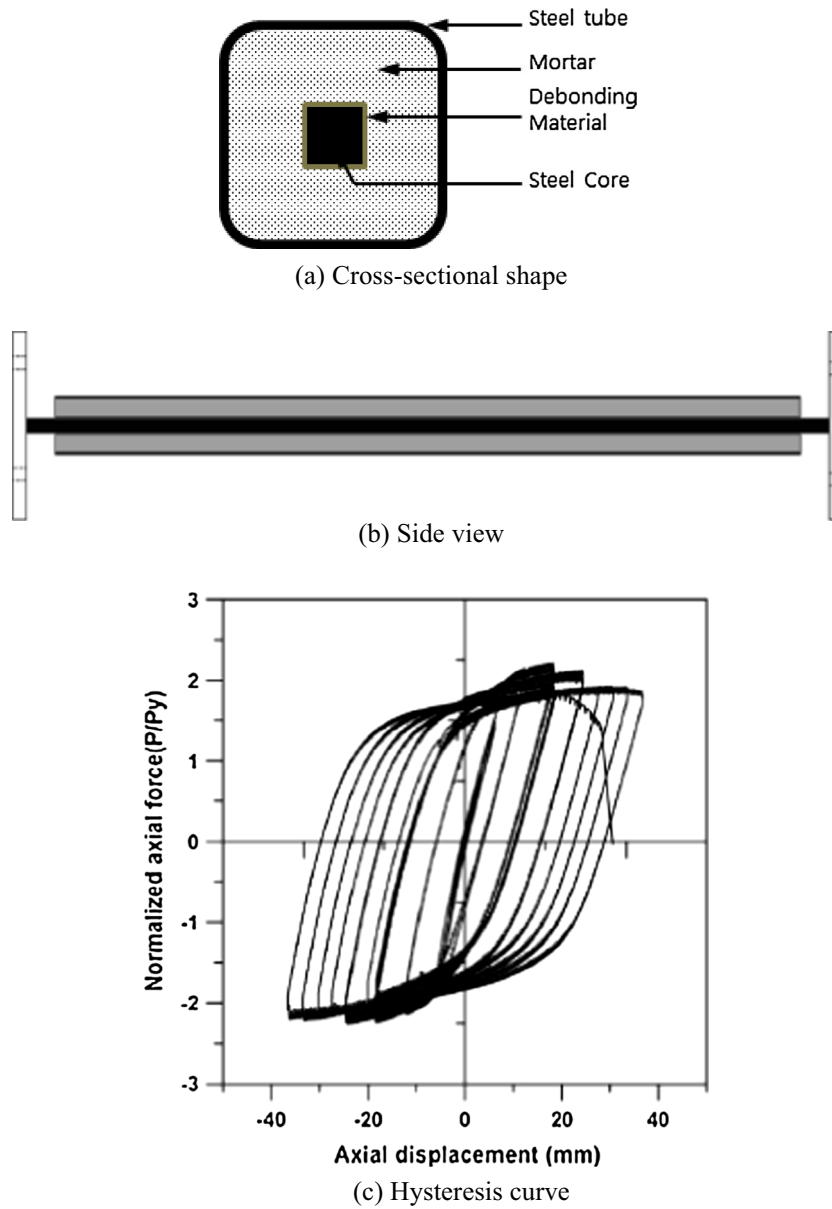
(a) Cross-sectional shape

(b) Side view

(c) Hysteresis curve

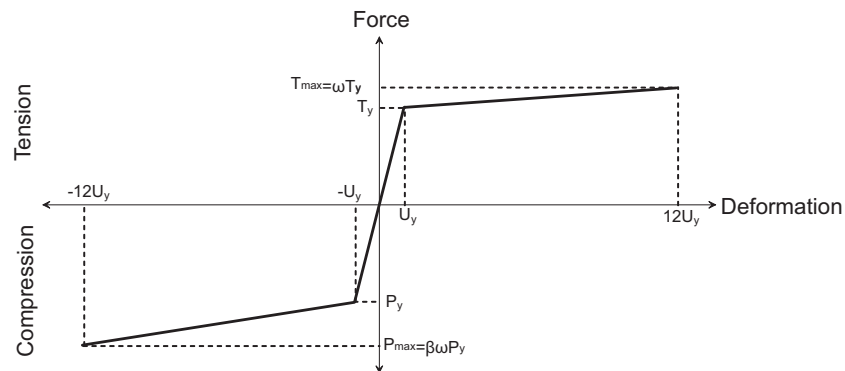**Fig. 21.** Buckling restrained brace used in the retrofit design.

Fig. 22. Idealized backbone curve of the BRB.
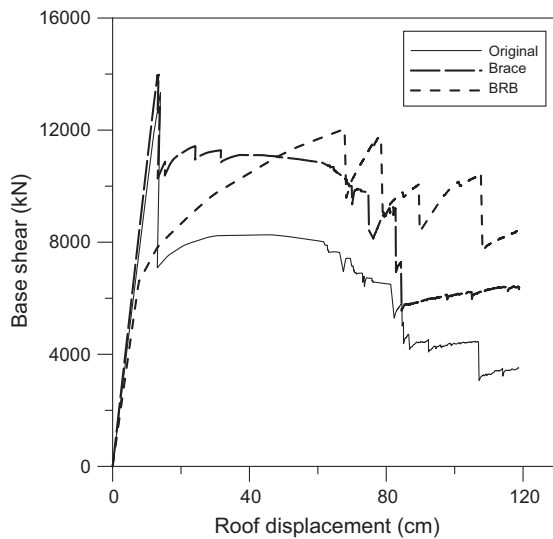
Fig. 23. Pushover curves of the Type B structures after retrofit.

Table 12
Overstrength and ductility factors of the retrofitted 12-story Type B structure.

|	δ_y (cm)	δ_u (cm)	μ	Ω
Original	14.02	49.69	3.54	7.32
Brace	13.45	54.18	4.03	7.67
BRB	12.42	68.29	5.50	6.60

(a) End bracing   (b) BRB

Fig. 24. Plastic hinge formation of the Type B structures after retrofit.

The inter-story drifts of the structures corresponding to the four different global damage states are presented in Table 13. The median structural capacities associated with each global limit
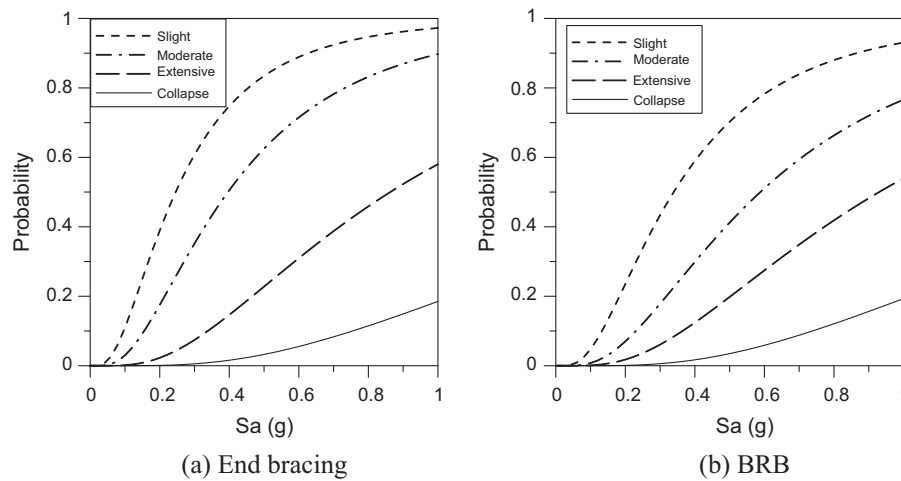
Table 13
Limit states for the maximum inter-story drift ratio of the retrofitted Type B structures at each damage state.

	Slight	Moderate	Extensive	Complete
Original	0.0026	0.0078	0.0146	0.0379
BRB	0.0053	0.0081	0.0190	0.0513
Brace	0.0025	0.0068	0.0149	0.0375

Table 14
Median structural capacity $\widehat{C}$ for the retrofitted Type B structures associated with the global limit states (g).

	Slight	Moderate	Extensive	Complete
Original	0.34	0.58	0.76	1.38
BRB	0.25	0.40	0.86	1.92
Brace	0.34	0.59	0.93	1.88

state, $\widehat{C}$, obtained from incremental dynamic analysis results are shown in Table 14. In the structure retrofitted with end bracing the median structural capacities associated with the Slight and the Moderate limit states are similar to those of the original structure. However the median capacities for the Extensive and Complete limit states are 1.2 and 1.3 times larger than those of the original structure. The median capacities of the structure retrofitted with BRB for the Slight and the Moderate limit states are smaller than those of the original structure. However the median capacities for the Extensive and Complete states are 1.1 and 1.4 times larger than those of the original structure. Fig. 25 depicts the fragility curves of the retrofitted model structures. In comparison with those of the original structure shown in Fig. 13, the seismic fragilities of the structure with additional end bracing for the Slight and the Moderate damage states rather slightly increased, whereas the fragilities for the Extensive and the Complete damage states slightly decreased. Similar probabilities of reaching the Slight and the Moderate damage states were observed in the structure retrofitted with BRB. However the fragilities for the Extensive and the Complete damage states further decreased compared with those of the structure retrofitted with end bracing. The analysis results show that, even though the BRB model has lower yield and maximum strengths, it displays quite ductile behavior with smaller probability of extensive damage and collapse. The scheme also has the advantage in that spatial planning is not interfered with addition of structural elements.

6. Concluding remarks

In this study the seismic performance of staggered truss system (STS) structures with and without vierendeel panels retrofitted with various schemes such as adding interior columns, vertical cables, end braces, and buckling-restrained braces (BRB). Pushover analyses were carried out to estimate the nonlinear load–displacement relationship, and the probabilities of reaching four damage states were obtained from incremental dynamic analysis results of 44 earthquake records.

The analysis results showed that the prototype STS structures had enough strength but limited ductility, and that the seismic performance of the STS could be enhanced with the proposed retrofit schemes. The seismic performance of the STS with vierendeel panels could be greatly increased by installing interior columns. The use of end bracing and vertical cable also turned out to be somewhat effective in enhancing strength and ductility of the STS with vierendeel panels, especially in the Collapse damage state. It was also observed that when vertical cables were
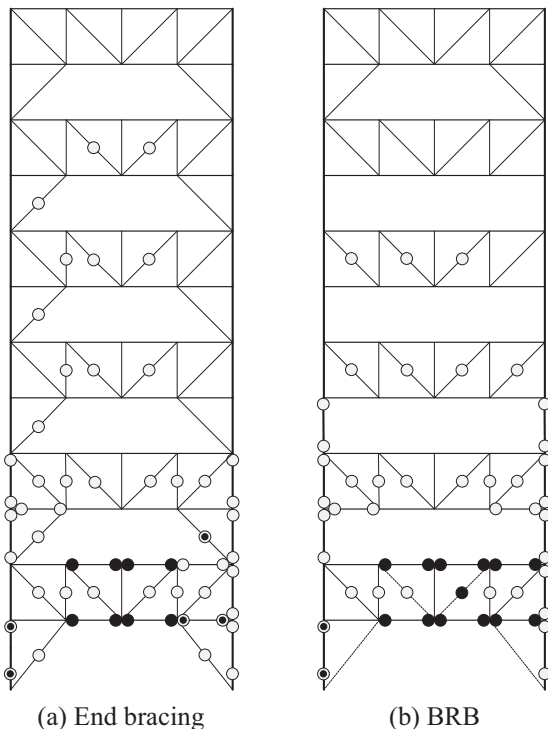
Fig. 25. Fragility curves of the retrofitted Type B structures.

installed along both sides of the vierendeel panels, plastic hinges were concentrated at the chord members of the vierendeel panels and were evenly distributed throughout the stories. Considering the fact that the addition of interior columns and end bracing will interfere with spatial planning of the building, the addition of cables, hidden inside of partition walls, may be an efficient option for enhancing seismic performance of STS structures. It was also noticed that the ductility of the STS structure without vierendeel panels could be enhanced by applying additional end bracing or replacing some of the critical diagonal members with BRB.

References

[1] Taranath BS. Steel, concrete, & composite design of tall buildings. McGraw Hill; 1998.
[2] Scalzi JB. The staggered-truss system-structural considerations. AISC Eng J 1971(October).
[3] Cohen MP. Design solutions utilizing the staggered-steel truss system. AISC Eng J 1986(third quarter).
[4] Kim J, Lee J, Kim Y. Inelastic behavior of staggered truss systems. Struct Des Tall Spec Struct 2007;16(1):85–105.
[5] Zhou XH, He YJ, Xu L, Zhou QS. Experimental study and numerical analyses on seismic behaviors of staggered-truss system under low cyclic loading. Thin Walled Struct 2009;47(11):1343–53.
[6] Chen CK, Zhang W. Experimental study of the mechanical behavior of steel staggered truss system under pool fire conditions. Thin Walled Struct 2011;49 (11):1442–51.
[7] Brazil A. Staggered truss system proves economical for hotels. Mod Steel Constr 2000(September).
[8] Mcknamara RJ. Aladdin Hotel. Modern Steel Construction, American Institute of Steel Construction; 1999.
[9] Pollak BS, Gustafson M. Complex apartments. Modern steel construction. American Institute of Steel Construction, Fall; 2004.
[10] AISC. Steel design guide 14: staggered truss framing system. Chicago, IL, USA: American Institute of Steel Construction; 2003.
[11] FEMA 450. NEHRP recommended provisions for seismic regulations for new buildings and other structures. Washington, D.C.: The Building Seismic Safety Council; 2003.
[12] Basha HS, Goel SC. Special truss moment frames with Vierendeel middle panel. Eng Struct 1995;17(5):352–8.
[13] Longo A, Montuori R, Piluso V. Theory of plastic mechanism control of dissipative truss moment frames. Eng Struct 2012;37:63–75.
[14] Wongpakdee N, Leelataviwat S, Goel SC, Liao WC. Performance-based design and collapse evaluation of buckling restrained knee braced truss moment frames. Eng Struct 2014;60:23–31.
[15] ASCE 7. Minimum design loads for buildings and other structures. American Society of Civil Engineers; 2010.
[16] AISC 360-10. Specification for structural steel buildings. Chicago, IL, USA: American Institute of Steel Construction.
[17] ASCE 41. Seismic rehabilitation of existing buildings. American Society of Civil Engineers; 2006.
[18] PERFORM-3D. Nonlinear analysis and performance assessment for 3D structures-user guide. Berkeley (CA, USA): Computers and Structures; 2006.
[19] FEMA P695. Quantification of building seismic performance factors. Federal Emergency Management Agency; 2009.
[20] PEER. PEER NGA database. Berkeley, U.S.A: Pacific Earthquake Engineering Research Center, University of California; 2006. <http://peer.berkeley.edu/nga/ >.
[21] HAZUS-MH 2.1. Technical Manual Federal Emergency Management Agency; 2010.
[22] Cornell CA, Jalayer F, Hamburger R, Foutch D. Probabilistic basis for 2000 SAC Federal Emergency Management Agency steel moment frame guidelines. J Struct Eng 2002.
[23] Park J, Lee J, Kim J. Cyclic test of buckling restrained braces composed of square steel rods and steel tube. Steel Compos Struct 2012;13:423–36.